Lab #4

DC Motor

MECHENG 552

Team 4B

Saptadeep Debnath
Manavendra Desai
Ellen Kim
David Radtke

Professor Shorya Awtar
8 November 2019

Department of Mechanical Engineering
University of Michigan, Ann Arbor

Contents

List of Figures

List of Tables

Table 1: Table of Symbols

Parameter	Symbol
The O coordinate system	O
The B coordinate system	B
Moment of Inertia	MoI
Center of Mass	CoM
Gravity	g
Length of Horizontal Arm	L_1
Distance Of Horiz. Arm CoM from Pivot	L_{11}
Mass of Horiz. Arm	M_1
MoI of the Horizontal Arm Assembly at its CoM and aligned with O	I_{1,O_Z}
Friction Torque for Direction θ	$T_{f,\theta}$
Viscous Damping for Direction θ	B_θ
Back EMF Constant for Motor	K_b
Torque Constant for Motor	K_t
Motor Resistance	R
Motor Inductance	L
Motor Viscous Damping Constant	B_m
Friction Torque for Motor	$T_{f,motor}$
Motor Inertia	J_m
Length of Pendulum Arm	L_2
Distance Of Pendulum Arm CoM from Pivot	L_{21}
Mass of Pendulum Arm	M_2
MoI of Pendulum at its CoM and aligned with B	I_{2,B_X}
MoI of Pendulum at its CoM and aligned with B	I_{2,B_Y}
MoI of Pendulum at its CoM and aligned with B	I_{2,B_Z}
Product of Inertia of Pendulum aligned with B_{XY}	$I_{2,B_{XY}}$
Friction Torque for Direction α	$T_{f,\alpha}$
Viscous Damping for Direction θ	B_α

1 System Modeling (40pts)

(a) Physical Model (5)

The physical model for the inverted pendulum system can be split into those for the D.C motor, links, driver and encoder.

Mechanical model for the D.C motor

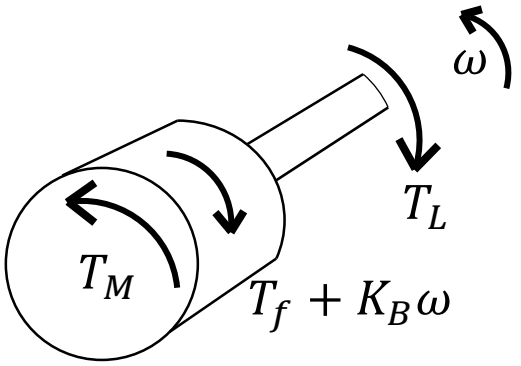

Figure 1: Lumped physical model for the mechanical aspects of the D.C motor

Figure 1 shows the free body diagram for the D.C motor. T_M is the torque available at the motor. $T_f + K_B\omega$ is the friction and viscous damping torque. They internally load the motor and reduce the torque available at the shaft. T_L is the load torque the motor must overcome while ω is the motor shaft speed.

Electrical model for the D.C motor

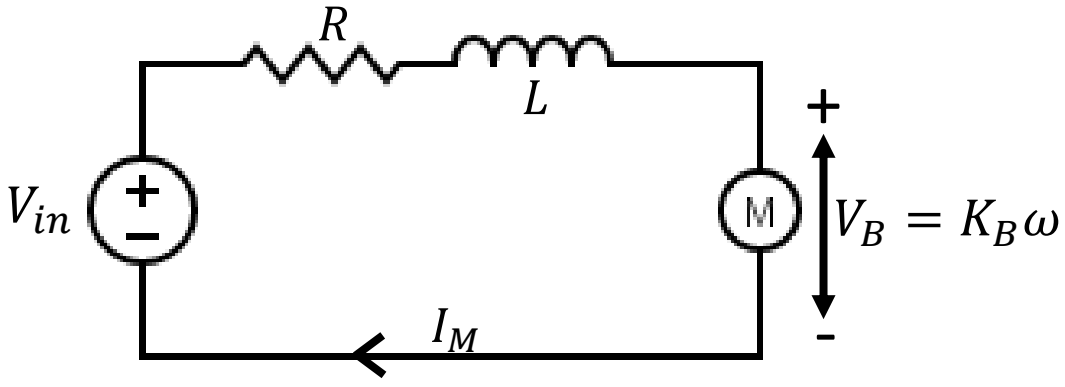

Figure 2: Lumped physical model for the electrical aspects of the D.C motor.

Figure 2 shows the simplified electric circuit diagram for the D.C motor. V_{in} is the voltage applied across the motor leads, by the servo amplifier. R and L are the motor resistance and inductance respectively. V_B is the back emf generated due to a motor shaft speed ω. I_M is

the resulting current in the motor.

Mechanical model for the links of the inverted pendulum

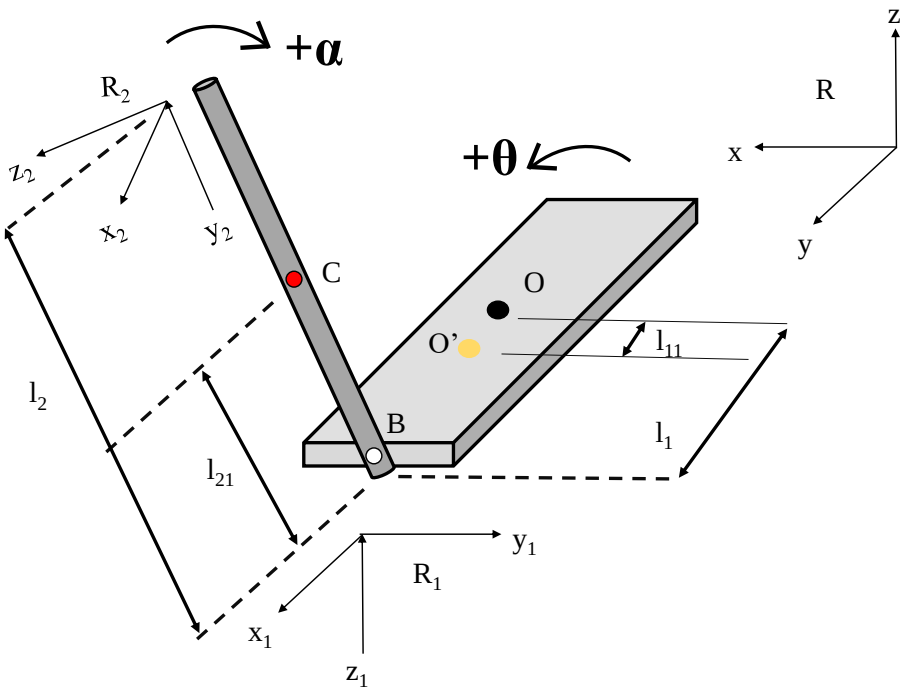

Figure 3: Physical model of the inverted pendulum links along with the chosen coordinate systems and rotation angle conventions.

A horizontal link of length l_1 rotates about pivot O. The angle rotated is θ, defined in the inertia frame R, taken positive in the anti-clockwise direction when looking from the top. O' denotes its centre of gravity, located a distance l_{11} from O. Attached to the horizontal link at pivot B is the pendulum link, of length l_2. It rotates an angle α in the frame R_1, which is fixed to the horizontal link. α is taken to be positive when rotating in the clockwise direction with us looking towards the centre of the motor. C denotes its centre of gravity, located a distance l_{21} from B. R_2 is the pendulum fixed coordinate reference frame.

Servo Amplifier

Since the actuator driver has a bandwidth of around 2.5 kHz, much larger than operating frequencies of the mechanical components of the inverted pendulum system, the gain K_a A/V remains unchanged and the driver is hence modelled as a constant gain block.

Encoders

Incremental encoders are used for to measure rotation angles for the horizontal link and the pendulum link. Both encoders give 500 counts per revolution of the D.C motor shaft and the pendulum link, while they send 2000 pulses each to myRio per revolution, on account of quadrature decoding. This results in an increased resolution of 0.18^o. When multiplied with the number of revolutions, we obtain the respective angles rotated.

(b) Assumptions (2)

Engineering assumptions made while developing the physical model for the inverted pendulum (IP) system are stated below - The D.C motor mechanical set-up:

1. The D.C motor shaft is rigid.
2. Lubricants contained in the motor behave as Newtonian fluids, hence their viscosity remains unchanged over our range of operation. Therefore, viscous damping is always proportional to motor speed.
3. Friction torques (static and dynamic) remain unchanged over our range of operation.

The D.C motor electrical system:

1. The resistance and inductance remain unchanged over our range of operation.
2. The magnetic field of the permanent magnets of the D.C motor remains unchanged over our range of operation.
3. The torque constant remains unchanged over our range of operation.
4. The slope of the Torque - Speed curve, i.e, the damping constant D (as given in the Pittman motor datasheet), remains unchanged over our range of operation.

The link set-up:

1. Links are assumed to be rigid since for the present operating conditions, loads on links (mainly centrifugal in nature) are not large enough to cause any bending of the links or distortion of the link at the respective pivots.
2. The IP system is a pure two degree of freedom system. Since all components are assumed to be rigid and tightly assembled, there is no added bending, twisting or slipping occurring at the time of operation that may add to the degrees of freedom of motion.
3. The pendulum is symmetric in the x_2y_2 plane in the R_2 frame.
4. Dynamic response of both encoders is fast enough to assume instantaneous angle measurement. This argument is based on the D.C motor lab exercises, wherein we observed the quantization step for the encoder to be sufficiently small and compliment the sampling frequencies (set by us) of myRio well.
5. Since the servo-amplifier has a bandwidth of ~ 2.5 kHz, it is assumed that its gain K_a A/V is unaffected by the system dynamics and thus remains unchanged over the range of frequencies of our interest (*O(1)* Hz). The driver is hence modelled as a constant gain block that provides instantaneous current output to a reference voltage input.
6. The added stiffness of the 6 foot long pendulum encoder cable (enter product name) is treated as an unmodelled disturbance from the environment on the plant and is therefore not accounted for in the equations of motion for the plant.

(c) Mathematical Model (5)

Equations of motion for the D.C motor

Equation of motion for the motor rotor relating the motor driving torque T_M and rotor position θ -

$$J\ddot{\theta} + B\dot{\theta} = T_M - T_L - T_f \tag{1}$$

In the absence of an external load at steady state, $\dot{\theta} = 0$ and $T_L = 0$. Therefore,

$$B\dot{\theta}_{ss} = T_{M,ss} - T_f$$

Equations in the electrical domain for the D.C motor

$$V_{in} - K_B\dot{\theta}_{ss} = I_M R + L\frac{dI_M}{dt} \tag{2}$$

At steady state,

$$V_{in} - K_B\dot{\theta}_{ss} = I_{M,ss}R = \frac{T_{M,ss}R}{K_T}$$

Combining Eq. 1 and Eq. 2, and writing in the s domain, V_{in} can be related to $\dot{\theta}$ (or ω) as follows -

$$\omega(s) = V_{in}(s)\left(\frac{K_T}{K_T K_B + (Js+B)(Ls+R)}\right) - T_f\left(\frac{Ls+R}{K_T K_B + (Js+B)(Ls+R)}\right) \tag{3}$$

$$\theta(s) = \frac{\omega(s)}{s} \tag{4}$$

Eq. 3 and Eq. 4 relate the inputs V_{in} and T_f(a disturbance) to the relevant outputs ω and θ. Any noise that may arise due to the quantization scheme of the encoder and the time discretized loop of myRio has been ignored.

Equations of motion for the pendulum links

The coordinate transformations used to write equations of motion for the links in R are shown below

$$\begin{bmatrix}\hat{i}_1\\ \hat{j}_1\\ \hat{k}_1\end{bmatrix} = \begin{bmatrix}\cos\theta & \sin\theta & 0\\ -\sin\theta & \cos\theta & 0\\ 0 & 0 & 1\end{bmatrix}\begin{bmatrix}\hat{i}\\ \hat{j}\\ \hat{k}\end{bmatrix} \;;\; \begin{bmatrix}\hat{i_2}\\ \hat{j_2}\\ \hat{k_2}\end{bmatrix} = \begin{bmatrix}1 & 0 & 0\\ 0 & \cos\phi & \sin\phi\\ 0 & -\sin\phi & \cos\phi\end{bmatrix}\begin{bmatrix}\hat{i_1}\\ \hat{j_1}\\ \hat{k_1}\end{bmatrix}$$

$\hat{i}, \hat{j}$ and $\hat{k}$ represent unit normal vectors in R, while the subscripts 1 and 2 correspond to R_1 and R_2 respectively.

Hamilton's principle and Lagrange's equations (energy based) are used to obtain the equations of motion. Since the horizontal link is constrained in the vertical direction, it will not contribute to changes in potential energy of the system, but will contribute to the kinetic energy of the system only. Also, the upright position of the pendulum link is considered

to be the reference for calculating V. Keeping this in mind, kinetic energy T and potential energy V of the system can be written as,

$$T = \frac{1}{2}m_1({}^R v^{O'})^2 + \frac{1}{2}\bar{I}_{1_{z_1}}(\dot{\theta})^2 + \frac{1}{2}m_1({}^R v^C)^2 +$$
$$\frac{1}{2}\left[\bar{I}_{2_{x_2}}(\dot{\phi})^2 + \bar{I}_{2_{x_2}}(\sin\phi)^2(\dot{\theta})^2 + \bar{I}_{2_{z_2}}(\cos\phi)^2(\dot{\theta})^2 + \bar{I}_{2_{x_2}}\bar{I}_{2_{x_2}}\dot{\theta}\dot{\phi}\sin\phi\right]$$

$$V = -m_2 g l_{21}(1 - \sin\phi)$$

Using **Hamilton's principle**, the generalized forces Q_θ and Q_ϕ for the horizontal and pendulum links are obtained as,

$$Q_\theta = T_M - B_\theta\dot{\theta} - T_{f,d\theta}sgn(\dot{\theta}) \tag{5}$$

$$Q_\phi = -B_\phi\dot{\phi} - T_{f,d\phi}sgn(\dot{\phi}) \tag{6}$$

$T_{f,d\theta}$ and $T_{f,d\theta}$ are the Coulomb friction at the D.C motor shaft and the pendulum encoder shaft respectively. Similarly, B_θ and B_ϕ are the viscous damping constants for the D.C motor shaft and encoder shaft respectively.
The **Lagrange's equation of motion** can be written as,

$$Q_\theta = \frac{d}{dt}\frac{\partial T}{\partial\dot{\theta}} - \frac{\partial T}{\partial\theta} + \frac{\partial V}{\partial\theta} \tag{7}$$

$$Q_\phi = \frac{d}{dt}\frac{\partial T}{\partial\dot{\phi}} - \frac{\partial T}{\partial\phi} + \frac{\partial V}{\partial\phi} \tag{8}$$

Using Eq. 5,6,7 and 8, we obtain the following non-linear equations of motion,
Horizontal link

$$\left[m_1 l^2{}_{11} + \bar{I}_{1_{z_1}} + m_2 l^2{}_1 + m_2 l^2{}_{21}(\cos\phi)^2\bar{I}_{2_{z_2}}(\cos\phi)^2 + \bar{I}_{2_{y_2}}(\sin\phi)^2\right]\ddot{\theta} + \tag{9}$$
$$\left[\bar{I}_{2_{x_2y_2}} - m_2 l^2{}_{21} - \bar{I}_{2_{z_2}}(2\cos\phi\sin\phi)\dot{\theta}\dot{\phi}\right] = \frac{d}{dt}\frac{\partial T}{\partial\dot{\theta}} - \frac{\partial T}{\partial\theta} + \frac{\partial V}{\partial\theta}$$

Pendulum link

$$\left[m_2 l^2{}_{21} + \bar{I}_{2_{x_2}}\right]\ddot{\phi} + \left[-m_2 l_1 l_{21} + \bar{I}_{2_{x_2y_2}}\right](\sin\phi)\ddot{\theta} + \left[m_2 l^2{}_{21} + \bar{I}_{2_{z_2}} - \bar{I}_{2_{y_2}}\right](\cos\phi)(\sin\phi)\dot{\theta}^2 \tag{10}$$
$$+ m_2 g l_{21}\cos\phi = \frac{d}{dt}\frac{\partial T}{\partial\dot{\phi}} - \frac{\partial T}{\partial\phi} + \frac{\partial V}{\partial\phi}$$

(d) Parasitic Effects (2)

The parasitic effect of Coulomb friction has already been incorporated in the plant dynamics. Also, based on LAB 3 D.C motor exercises, the quantization step size of the encoders are sufficiently small and compliment the LabVIEW simulation parameters well to give a reasonable output for angles.

(e) Simulink Non-linear Model (10)

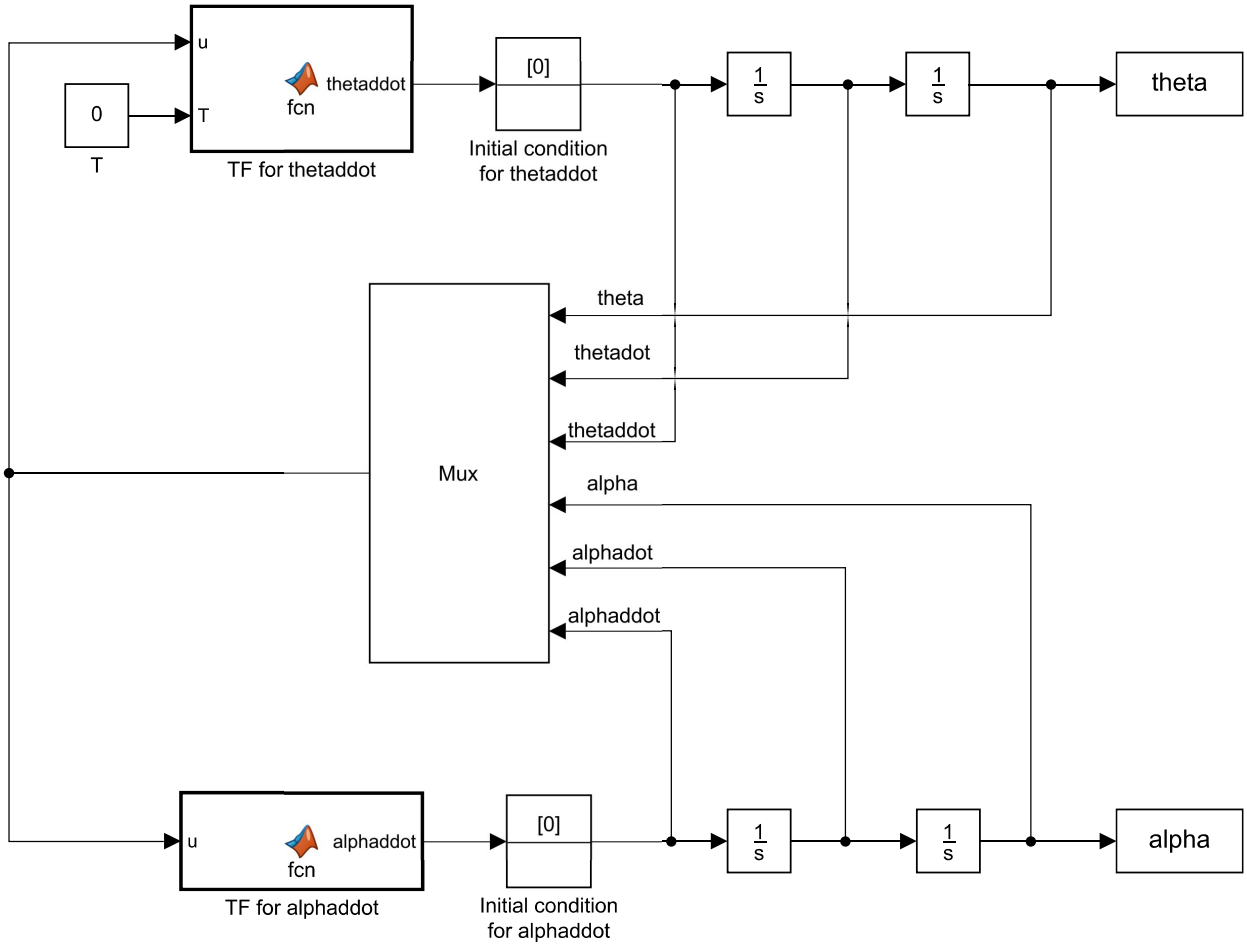

Figure 4: Open Loop Non-linear Block Diagram. The transfer functions for the non-linear systems are defined in the two MATLAB function blocks. Additional initial condition blocks are added to both the branches of θ and α to initialise $\ddot{\theta}$ and $\ddot{\alpha}$ as zero.

The non-linear equations stated in Eq. 9 and 10 are further modeled in Simulink as shown in figure 4.

(f) Linearization (6)

The non-linear equations (Eq. 9 and Eq. 10) are linearised about the operating point, which is set at $\theta = 0$ and $\alpha = 0$, which yields the following equations,

$$[m_1 l_{11}^2 + \bar{I}_{1_{z1}} + m_2 l_1^2 + \bar{I}_{2_{y2}}]\ddot{\theta} - [\bar{I}_{2_{x2y2}} - m_2 l_1 l_{21}]\ddot{\alpha} = T - B_\theta \dot{\theta}$$

$$-[m_2 l_{21}^2 + \bar{I}_{2_{x2}}]\ddot{\alpha} + [\bar{I}_{2_{x2y2}} - m_2 l_1 l_{21}]\ddot{\theta} + m_2 g l_{21}\alpha = B_\alpha \dot{\alpha}$$

These equations are further simplified as,

$$C_1\ddot{\theta} + C_2\ddot{\alpha} = T - B_\theta\dot{\theta}$$

$$C_3\ddot{\alpha} + C_2\ddot{\theta} - C_4\alpha = -B_\alpha\dot{\alpha}$$

where, $C_1 = m_1 l_{11}^2 + \bar{I}_{1_{z1}} + m_2 l_1^2 + \bar{I}_{2_{y2}}$,
$C_2 = m_2 l_1 l_{21} - \bar{I}_{2_{x2y2}}$,
$C_3 = m_2 l_{21}^2 + \bar{I}_{2_{x2}}$,
$C_4 = m_2 g l_{21}$

The linear model can be parametrically represented in either a transfer function or the state-space form.

Transfer Functions

$$\frac{\theta}{T} = \frac{C_3 s^2 + B_\alpha s - C_4}{(C_1 C_3 - {C_2}^2)s^4 + (B_\alpha C_1 + B_\theta C_3)s^3 + (B_\alpha B_\theta - C_1 C_4)s^2 - B_\theta C_4 s}$$

$$\frac{\alpha}{T} = \frac{-C_2 s^2}{(C_1 C_3 - {C_2}^2)s^4 + (B_\alpha C_1 + B_\theta C_3)s^3 + (B_\alpha B_\theta - C_1 C_4)s^2 - B_\theta C_4 s}$$

State-Space Equations

$$\begin{bmatrix} \dot{x}_1 \\ \dot{x}_2 \\ \dot{x}_3 \\ \dot{x}_4 \end{bmatrix} = \begin{bmatrix} 0 & 1 & 0 & 0 \\ 0 & \frac{-B_\theta C_3}{C_1 C_3 - {C_2}^2} & \frac{-C_2 C_4}{C_1 C_3 - {C_2}^2} & \frac{B_\alpha C_2}{C_1 C_3 - {C_2}^2} \\ 0 & 0 & 0 & 1 \\ 0 & \frac{B_\theta C_2}{C_1 C_3 - {C_2}^2} & \frac{C_1 C_4}{C_1 C_3 - {C_2}^2} & \frac{-B_\alpha C_1}{C_1 C_3 - {C_2}^2} \end{bmatrix} \begin{bmatrix} x_1 \\ x_2 \\ x_3 \\ x_4 \end{bmatrix} + \begin{bmatrix} 0 \\ \frac{C_3}{C_1 C_3 - {C_2}^2} \\ 0 \\ \frac{-C_2}{C_1 C_3 - {C_2}^2} \end{bmatrix} \begin{bmatrix} T \end{bmatrix} \tag{11}$$

The state-space equation (Eq. 11) is of the form $\dot{x} = Ax + Bu$, where the input to the system $'u'$ is the motor torque (T). The A and B matrices are defined as,

$$A = \begin{bmatrix} 0 & 1 & 0 & 0 \\ 0 & \frac{-B_\theta C_3}{C_1 C_3 - {C_2}^2} & \frac{-C_2 C_4}{C_1 C_3 - {C_2}^2} & \frac{B_\alpha C_2}{C_1 C_3 - {C_2}^2} \\ 0 & 0 & 0 & 1 \\ 0 & \frac{B_\theta C_2}{C_1 C_3 - {C_2}^2} & \frac{C_1 C_4}{C_1 C_3 - {C_2}^2} & \frac{-B_\alpha C_1}{C_1 C_3 - {C_2}^2} \end{bmatrix}, B = \begin{bmatrix} 0 \\ \frac{C_3}{C_1 C_3 - {C_2}^2} \\ 0 \\ \frac{-C_2}{C_1 C_3 - {C_2}^2} \end{bmatrix}$$

The output equation given as $y = Cx + Du$, depends on the outputs chosen by the user, which in this case is chosen to be the states of the system, i.e $'x'$. Therefore, C and D matrices are given as,

$$C = \begin{bmatrix} 1 & 0 & 0 & 0 \\ 0 & 1 & 0 & 0 \\ 0 & 0 & 1 & 0 \\ 0 & 0 & 0 & 1 \end{bmatrix}, D = \begin{bmatrix} 0 \end{bmatrix}$$

(g) Simulink Linear Model (10)

The state-space equations stated in Eq. 11 are further modeled in Simulink as shown in figure 5.

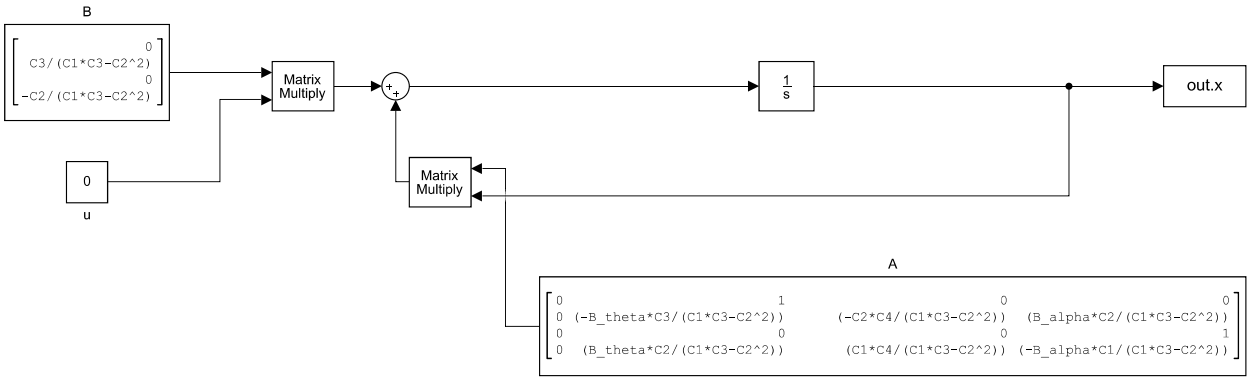

Figure 5: Open Loop Linear Block Diagram. The block diagram represents the equation $\dot{x} = Ax + Bu$ and is sufficient for the defined system, as the output $'y'$ is same as the states of the system $'x'$.

2 System Parameter Identification (15pts)

Table 2: System Parameters

Symbol	Value	Unit	Method
g	9.81	$\frac{m}{s^2}$	Constant
L_1	0.20	m	CAD
L_{11}	0	m	CAD
M_1	0.17	kg	Measured
I_{1,O_Z}	7.28E-4	$kg * m^2$	Experimental
$T_{f,\theta}$	1.98E-3	Nm	Experimental
B_θ	0	$\frac{Nms}{rad}$	Experimental
K_b	4.24E-2	$V\frac{s}{rad}$	Datasheet
K_t	4.24E-2	$\frac{Nm}{A}$	Datasheet
R	1.85	Ω	Datasheet
L	1.97E-3	H	Datasheet
B_m	3.7E-6	$\frac{Nms}{rad}$	Datasheet
$T_{f,motor}$	5.6E-3	Nm	Datasheet
J_m	8.5E-6	$kg * m^2$	Datasheet
L_2	0	m	Measured
L_{21}	0.08	m	CAD
M_2	0.08	kg	CAD
I_{2,B_X}	3.6E-4	$kg * m^2$	CAD
I_{2,B_Y}	3.7E-4	$kg * m^2$	CAD
I_{2,B_Z}	9.3E-6	$kg * m^2$	CAD
$I_{2,B_{XY}}$	0	$kg * m^2$	CAD
$T_{f,\alpha}$	2.75E-4	Nm	Experimental
B_α	2.10E-4	$\frac{Nms}{rad}$	Experimental

3 Linear Operation Range (10pts)

To test the parameters that have been identified in the previous section, the change in pendulum link angle α and in horizontal link angle θ are measured and compared with the nonlinear and linear simulation results from Simulink and are shown in figure 6 and 7.

Experimentally, it is shown that once the pendulum begins to fall from its top position, it will swing at the bottom center area until it stabilizes. Thus, in figure 6, the experimental values oscillate between the π or $-\pi$ radians. The nonlinear simulation shows a very close match to the experimental values and also stabilize. Initially, using the parameters found in previous section, the nonlinear simulation took longer than experimental values to stablize. Thus, to meet the experimental results, the $T_{f\alpha}$ was multiplied by 1.5 to increase friction, to dampen the system. The difference between the experimental parameter results may be due to the experimental fine tuning of the friction values. As the friction values were calculated

by taking the angle peaks at the decayed range, the value can easily vary depending on at what location the angle peaks were taken into consideration. The linear simulation results, on the other hand, shows to follow the initial angle drop up to approximately -0.4 radians; however, it fails to predict the oscillation about the bottom-center region and predicts to continuously turn. This is due to the pendulum angle exceeding the linearized range. Since the pendulum continues to swing, the figure 6 was created with no normalization to reduce the background noise. However, if normalized, it is expected to see a monotonic relationship between angle and time.

For the angle of horizontal link, the results in figure 7 shows the horizontal link swining in decaying oscillation until the pendulum stabilizes. The experimental and nonlinear simulation show the same frequency; however, the nonlinear predicts the horizontal link to oscillate at negative angle, while the experiment oscillated at positive angle. The difference between the two situations may be due to unmodeled dynamics. One of the components that we have not considered during simulation is the impact of the pendulum encoder wire's stiffness. Due to the encoder wire, the experimental set up had a bias in its direction and may have cause the experiment to diverge from the simulation results. The linear simulation results also show a good match up to θ of 0.4 radians; however, once it exceeds the linear range, it blows up and expects the horizontal link to continuously swing, similar to the pendulum link. This experiment clearly shows that the linear model should only be considered up to approximately ± 0.4 radians and is valid at this range.

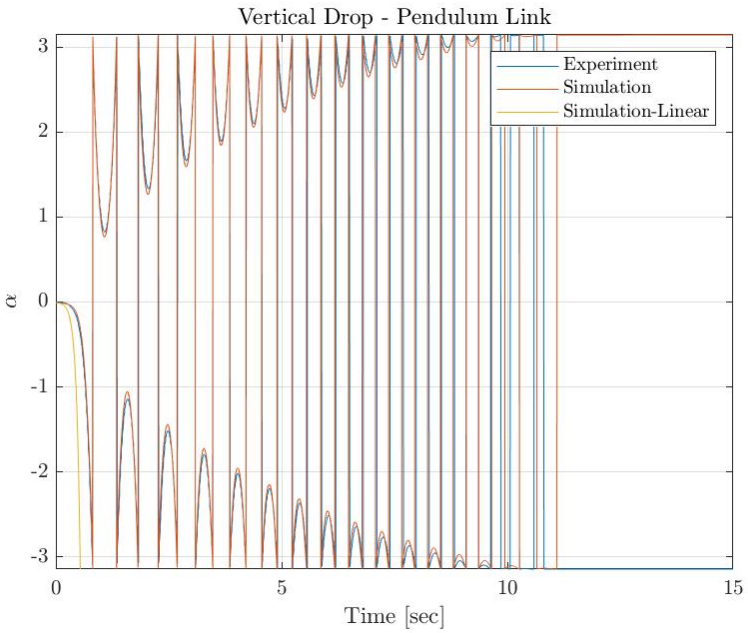

Figure 6: Vertical Drop - Pendulum. The change in angle of pendulum as it falls from the almost-balanced position is provided to compare nonlinear and linear simulations against the experimental results. The pendulum angle is normalized to $\pm\pi$ for the nonlinear simulation and experimental results. The linear fails to stabilize back to the original pendulum position (at the bottom-center) and predicts the pendulum to continue swinging. To reduce the noise in the background, the linear simulation results were not normalized, and they can be expected to continuously rotate.

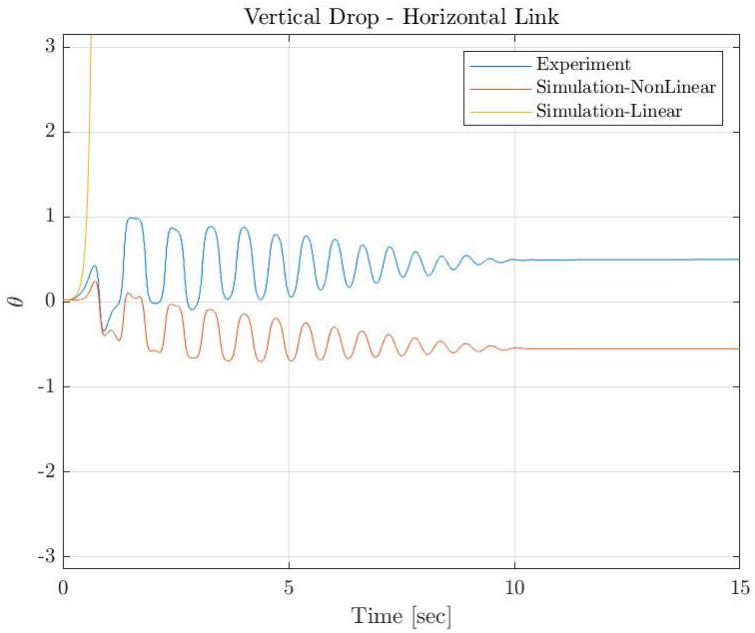

Figure 7: Vertical Drop - Horizontal Link. The change in angle of horizontal arm as the pendulum falls from the almost-balanced position is measured and compared with the linear and nonlinear simulation results.

4 Balancing Controller Design - State Space Approach (16pts)

(a) Block Diagram (3)

The mechatronic system block diagram of the linearized system model for closed-loop control system is shown below. This block diagram also shows the controller that is later implemented.

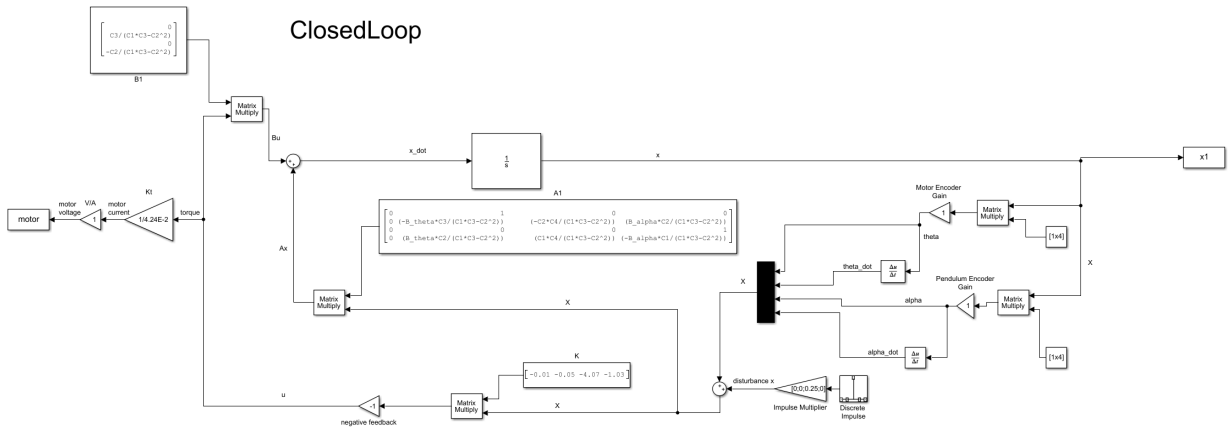

Figure 8: Block Diagram of Linear Model of Cloosed Loop System with Balancing Controller

(b) LQR Gains (5)

The full state feedback was implemented on the linearized model. The gains for full state feedback are calculated using the LQR function in MATLAB. The Q matrix represent the weight of importance of each of the states and the R matrix represent the weight of importance of the input. Our goal for the project is to implement an inverted pendulum where α is equal or close to 0 and $\dot{\alpha}$ should also equal or close to 0 for α requirement to meet. To obtain this goal, R is first applied at 100 because it is important for the torque input from the motor to have a relative high importance so that the horizontal link and pendulum link turns correctly and with correct magnitude. Additionally for the Q matrix, α is considered the most important, then $\dot{\alpha}$, $\dot{\theta}$, and lastly $\theta.\dot{\theta}$ is considered third most important because the horizontal link's velocity impact α and $\dot{\alpha}$. On the otherhand, the position of the horizontal link is the least important and it has not impact on accomplishing our goal. With this sequence in consideration, the values are distributed with approximatley an order of 10. There is a larger gap between the $\dot{\alpha}$ and $\dot{\theta}$ because we belived that α and $\dot{\alpha}$ control was more important than the horizontal link angle control. Thus, the LQR gain values calculated are shown in 3.

Table 3: Q and R matrices used to calculated LQR Gains.

Variables	Values
Q_θ	0.01
$Q_{\dot{\theta}}$	0.1
Q_α	1000
$Q_{\dot{\alpha}}$	100
R	100
K_θ	0.01
$K_{\dot{\theta}}$	0.05
K_α	4.07
$K_{\dot{\alpha}}$	1.03

(c) Controller Performance Simulation (13)

The LQR gains calculated was implemented in the linear and non-linear simulation models. The balancing controller's performance was tested in linear and non-linear model simulation for two scenarios: starting from non-zero position and injecting disturbance in balanced state. The response of the simulation results are shown in figure 9 and 10. Even when the position is set to 0.5 radians, both the linear and nonlinear models are able to have the system balance and show a very close to fit to each other. When an angular velocity disturbance of 0.25 radians is injected at 5 second, the system is able to balance the pendulum except that the non-linear model predicts oscillations about 0, while the linear model predicts stabilization with no oscillation. The impact of disturbance is more pronounced in the non-linear model. The linear model does not match the non-linear model due to the large angular velocity that exceeds its linearized range of operation. However, for both the scenarios, the controller can stabilize.

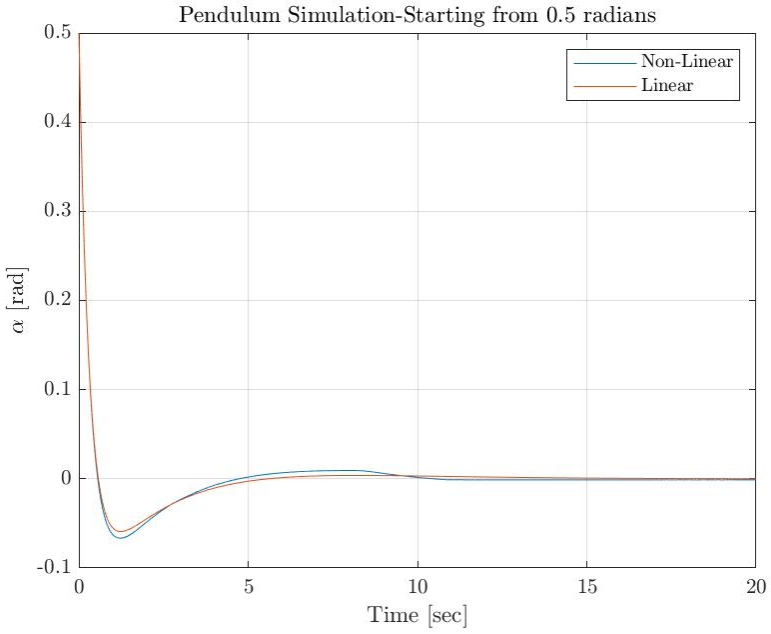

Figure 9: Balancing Controller Performance at Non-Zero Starting Position. The pendulum's initial angular position is set to 0.5 radians for the linear and non-linear models. Both the simulations show that the controller is able to stabilize the system

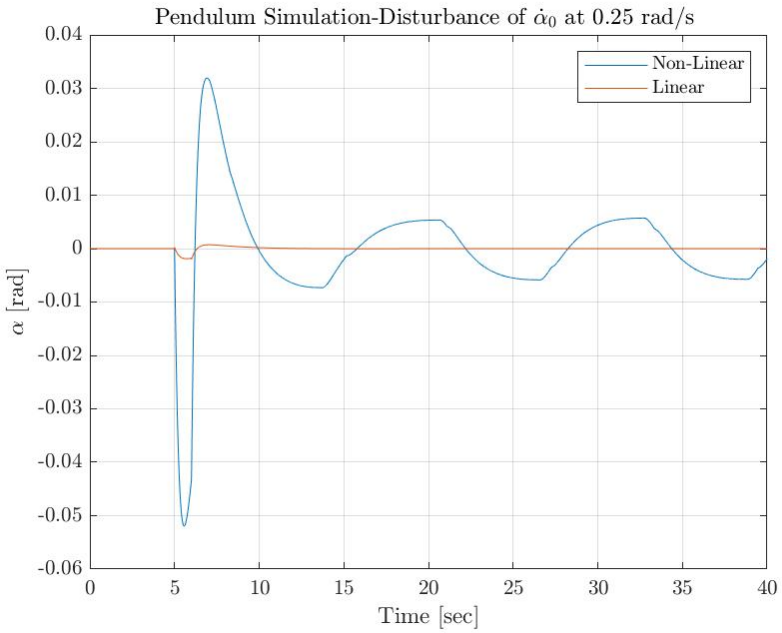

Figure 10: Balancing Controller Performance with Disturbance. The pendulum's angular velocity at 5 seconds was set to 0.25 rad/s. The linear model stabilizes, while the non-linear model shows oscillations around α equal to 0 with amplitude of 0.005 radians.

5 Swing-up Controller Design — Energy Approach (10pts)

For a pendulum that start in the vertically down position, we implement a controller to swing the pendulum to the linearized region, where the balancing controller takes effect, and ultimately has the pendulum in the vertically up position. The swing-up controller was designed using the energy approach. The controller calculates the total system energy based on the kinetic and energy of the horizontal and pendulum links and the potential energy of the pendulum. The calculated total system energy is compared with the energy of system at desired position, which is zero for the vertically balanced pendulum. The objective of this controller is insert energy to the system to force it out of the stable equilibrium to unstable equilibrium. This relationship is described by

$$V_{command} = K_A(E - E_0)sgn(\frac{d\alpha}{dt}cos(\alpha))$$

where K_A is the controller gain and E is the energy of the system. The controllers were implemented so that the swing-up controller is off within $\pm$ 25 degrees and balancing controller is on when pendulum is within $\pm$ 20 degrees. The swing-up controller gain was found through trial and error and its final gain for the below simulation results is 200. The higher the swing-up controller gain, the more aggressive the system inputs energy into the system. The figure 11 and 12 show the swing up and balancing controller in act as the pendulum starting at vertically down position ends up in the vertically up position. It is shown that the pendulum is able to stabilize in 4 swings of the pendulum link through various swings

in the horizontal link. Once the pendulum assumes the vertically up position, there are small fluctuations and the horizontal link gradually changes in its rotation to maintain the position.

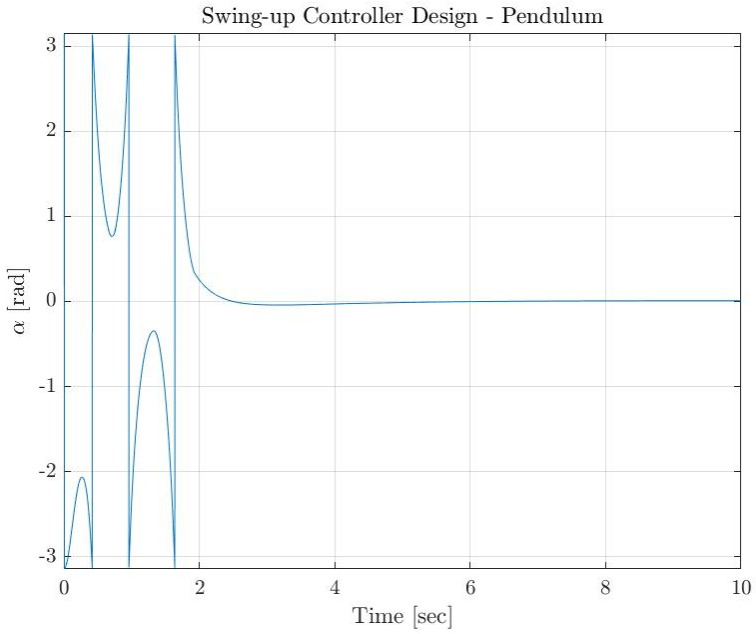

Figure 11: Swing-up Controller of Pendulum Link. The pendulum starts at the vertically down position and ultimately ends up in the vertically up position through the swing-up and balancing controllers.

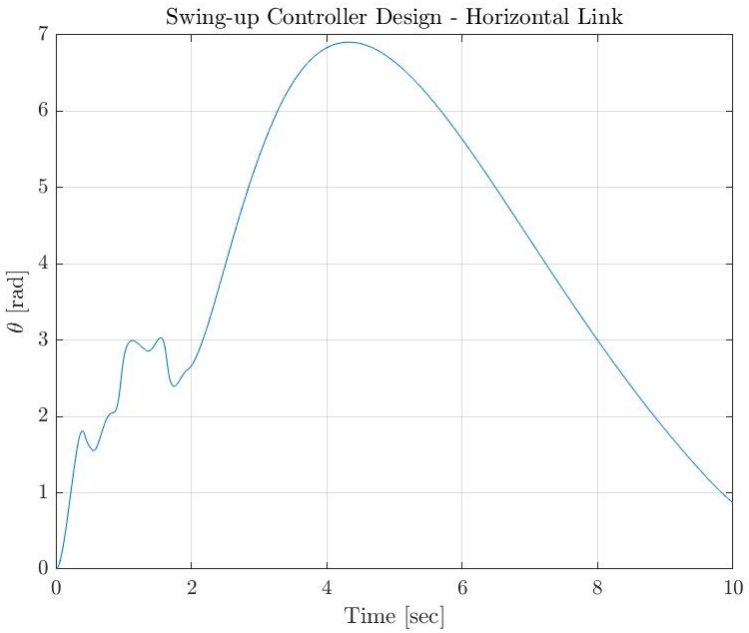

Figure 12: Swing-up Controller of Horizontal Link. The pendulum starts at the vertically down position and ultimately ends up in the vertically up position through the swing-up and balancing controllers.

6 Controller Implementation (22pts)

(a) LabVIEW Program (7)

The designed controllers were implemented in LabVIEW. The pendulum angle was normalized by

$$\alpha = \alpha - 2\pi floor\Big(\frac{\alpha + \pi}{2\pi}\Big)$$

where $floor(x)$ is a function to rounds x toward negative infinity. For the pendulum angle to operate within $\pm\pi$, the non-normalized angle is subtracted by 2π depending on if the non-normalized angle is equal or greater than π. This if-or condition allows the normalization. A screenshot of the normalization block diagram is shown below. Normalization of the pendulum link is necessary so that the direction of motor torque is correct. The pendulum angle can be in the 0 to 2π region; however, it would require additional calculations to decipher if the pendulum needs to rotate clockwise or counterclockwise.

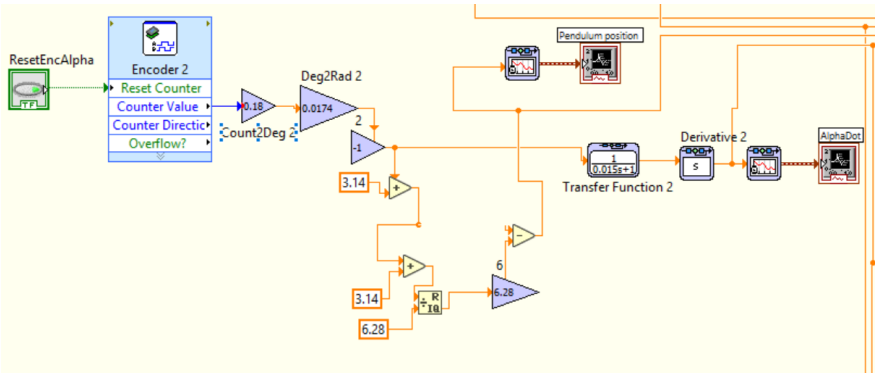

Figure 13: Normalization of Pendulum angle shown through Block Diagram

The overall block diagram of the LabVIEW VI is given by the figures below.

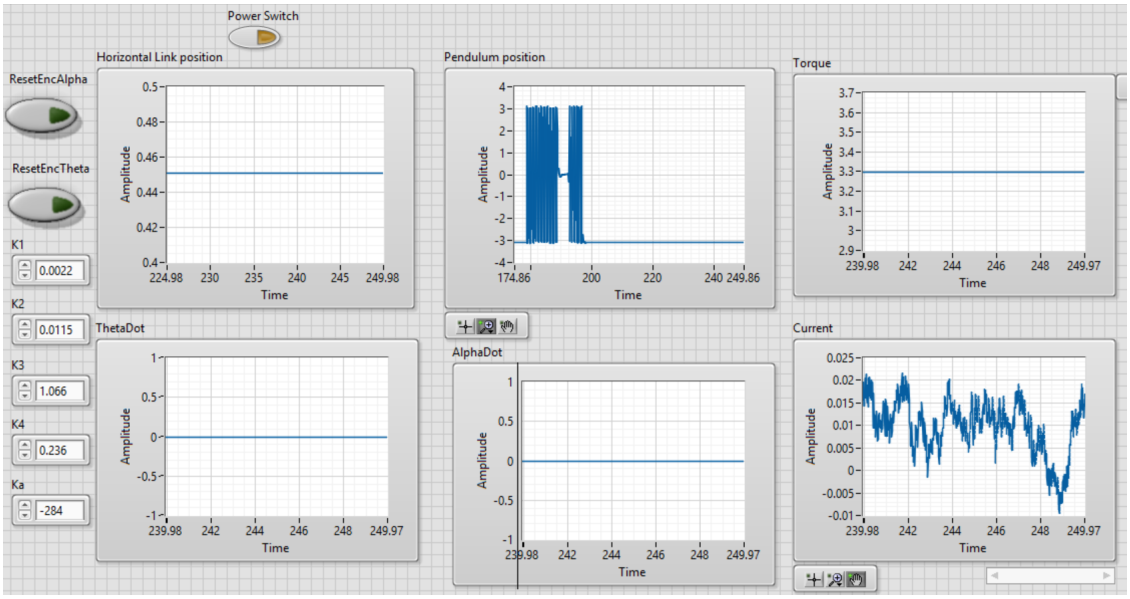

Figure 14: Front Panel of LabVIEW with both Controllers

IPsystem.vi
J:\ME552B\LAB4\LabVIEW\IPsystem.vi
Last modified on 11/6/2019 at 10:17 PM
Printed on 11/6/2019 at 10:27 PM

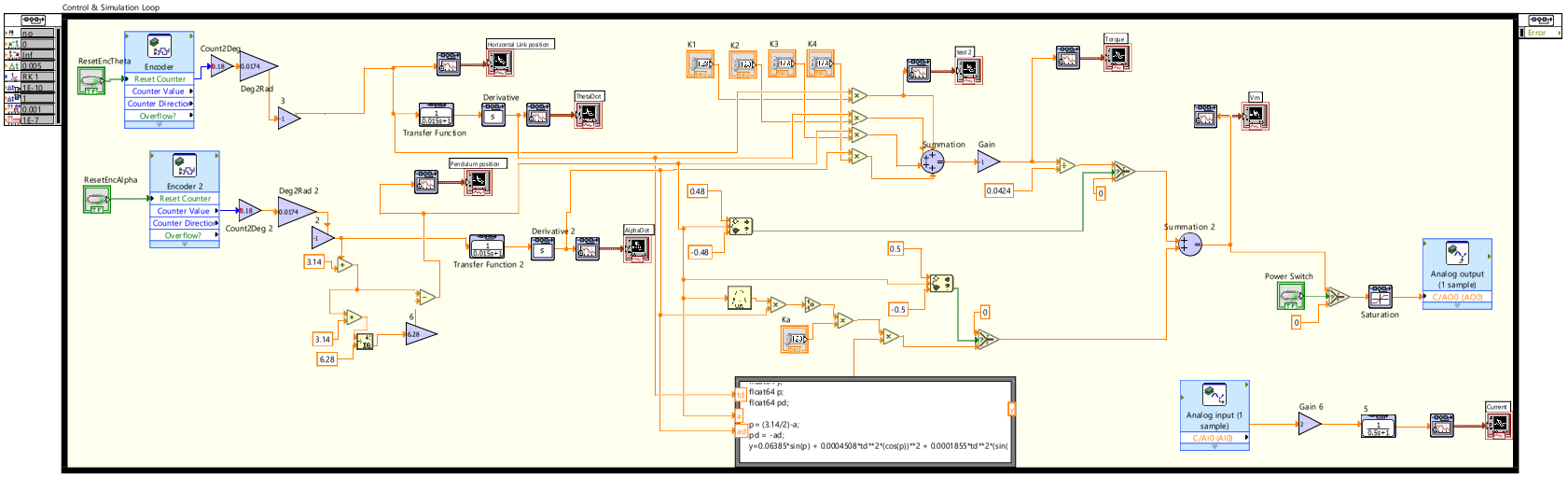

Figure 15: Block Diagram of LabVIEW with both Controllers

(b) Controller Performance (5)

With the desinged controllers implemented in LabVIEW, the experimental results from the swing-up and balancing controller were measured and shown in figure 16 and 17. The experimental operation range for the balancing controller was expanded to ± 0.48 radians and the swing-up controller will turn off if within $\pm$ 0.5 radians. The operation range for the balancing controller was expanded because the balancing controller has strong control than the swing-up controller and can balance the controller started at 0.5 radians. The deadband was also decreased so that the balancing controller will come into effect faster. With these changes, the experimental swing-up controller takes 5 swings for the pendulum to reach the balancing controller range and the balancing controller is able to stabilize around vertically up position within one second. The simulation results predicted that the controller would be able to achieve the swing-up in 4 swings. The difference may be due to again, the stiffness of the pendulum wire that is not accounted for and the parameter precision errors; however, the difference is quite small. The swing-up controller results are similar to the simulated swing-up controller results. The change in horizontal link angle is also shown and reflects that of the simulation results, where during swing-up, it makes smalll and fast rotations to increase pendulum swing amplitude and has a gradual rotation during balancing.

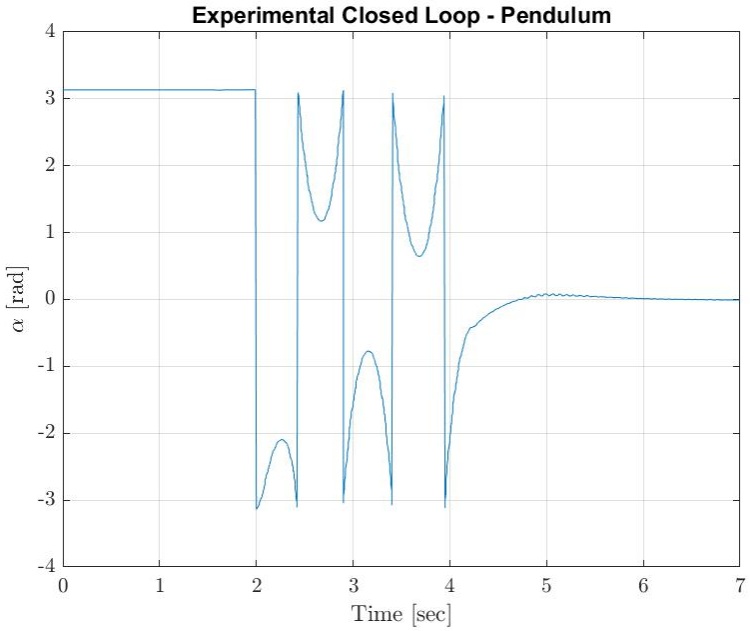

Figure 16: Experimental Swing-up and Balancing Controller - Pendulum

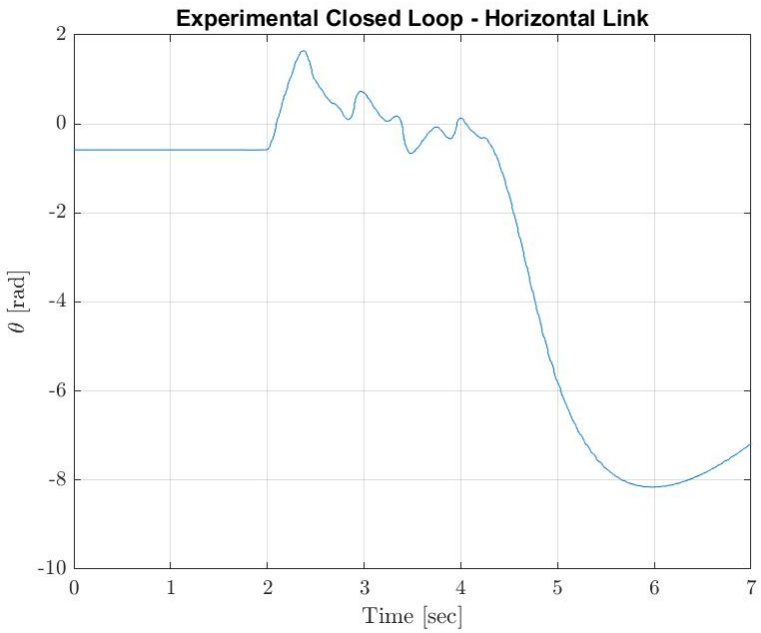

Figure 17: Experimental Swing-up and Balancing Controller - Horizontal Link

Additionally, the balancing controller's performance was tested experimentally through the same two scenarios of starting at non-zero location and injecting a disturbance in the balanced state. Figure 18 show 2 main peaks at 0.5 and 3 seconds. The experiment began with the letting the pendulum drop before turning on the motor. Thus, there is an initial drop to approximately -0.3 radians before the pendulum changes direction and balances the system again. Approximately at 3 seconds, the pendulum weight, in its balanced state, was tapped and shows sudden increase in angle due to disturbance. The controller was again able to overcome the disturbance and balance the system as it heads toward the vertically up position.

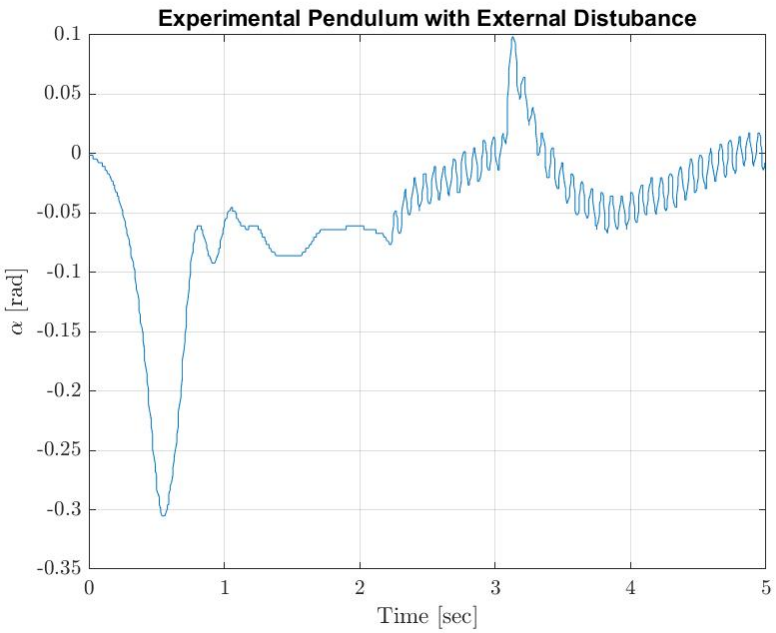

Figure 18: Experimental Balancing Controller with Disturbances

(c) Controller Robustness (10)

Now that the controllers implemented in LabVIEW are fully functional, the system configuration was varied to test the controllers' robustness. Firstly, the location/number of pendulum weight was varied. The experiment was separated to test the limits of the two controllers. For reference, the two pendulum weights have bend placed at the end of the rod at 5.75" and 6" from the rectangular bracket holding rod. Figure 19 shows the results when the one of the mass was displaced from its original location by 0.5" and compares it to its weights at the original location. Up to the 0.5" displacement, the system is able to perform swing-up and balancing of the pendulum. However, once the m_1 diverges further or one of the weights is taken off, the system is unable to perform swing-up. On the otherhand, to test the robustness of the balance controller, the location and number of pendulum weights were varied and tested when the pendulum was released from almost-balancing state. The test included, varying location of m_1 along the entire length of the rod while fixing location of m_2 and varying location of m_1 along the rod with m_2 removed from the system. For all these scenarios, it was able to maintain its balance controller, indicating a very robust balancing controller.

Varying Location of Pendulum Weight - Swing-up and Balance Controller

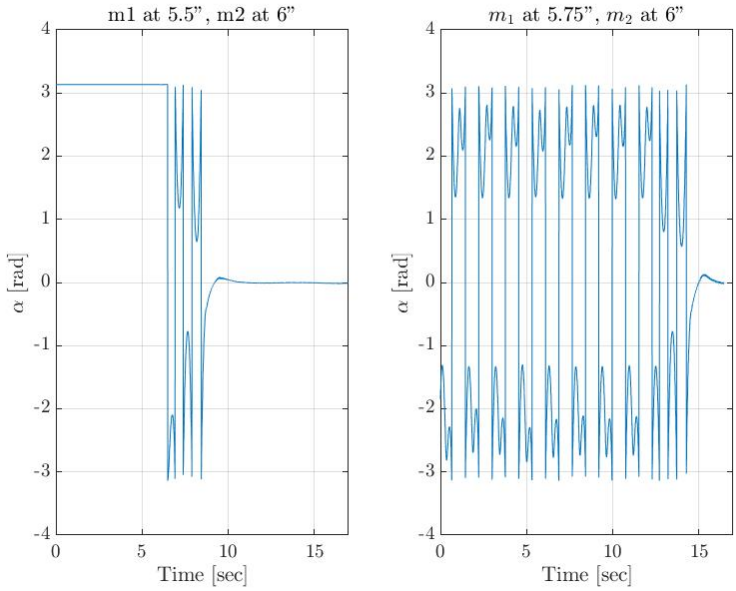

Figure 19: Varying location of pendulum weight - Swing-up and Balance Controller. The impact of varying the location of pendulum weight was analyzed by changing the location of the pendulum weights for a fully controlled system. The system was only able to balance when the m_1 was displaced by 0.5" from its original location (end of the link). When the masses are displaced further or removed, the system is unable to perform swing-up.

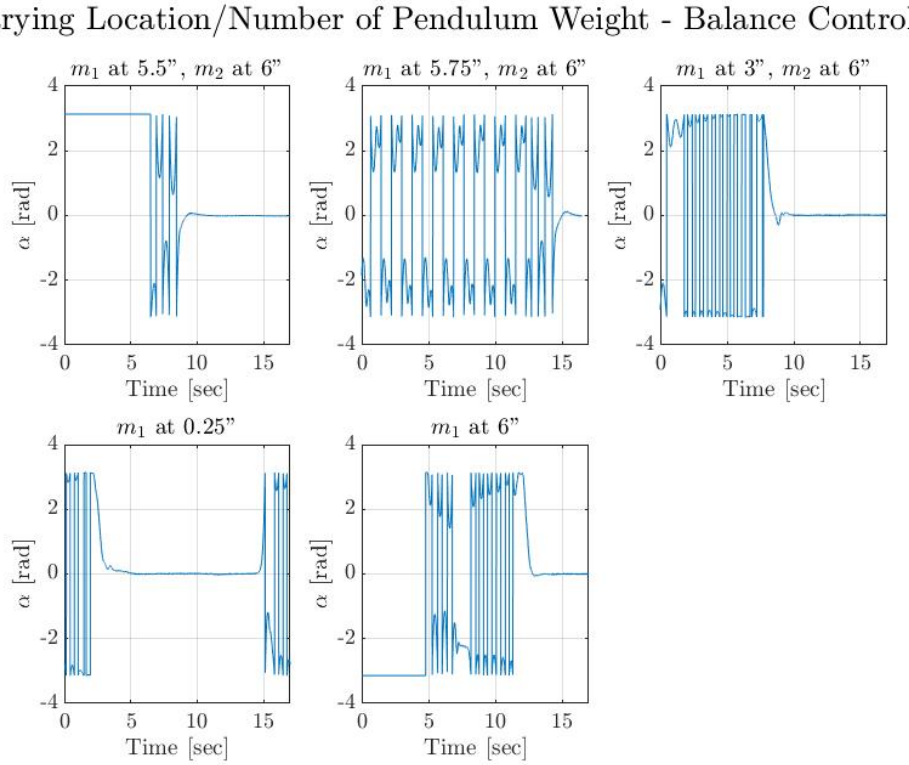

Figure 20: Varying location/number of pendulum weight for Balance Controller only. The impact of varying the location of pendulum weight was analyzed by changing the location with both weights on the rod and with only one weight. For all situations, the system was capable of continuously balancing the system

Additionally, to further test the controller robustness, the location of the ocunter weight was varied. The original position of the counterweight was 2cm from the end of the horizontal link and the counterweight is able to move from 0 to 5cm from the end of the horizontal link. The swing-up controller was able to achieve swing-up when the counter weight varied from 0 to 2cm from end of horizontal link as shown in figure 21. The balance controller on the other hand was able to achieve balancing control from 0 to 5cm from end of the horizontal link, where 0 and 5cm represent the maximum displacement range of the counter weight. Again, variance in counter weight location shows that the swing-up controller is capable of adequate changes in counter weight location, while the balance controller is capable of balancing despite the changing counter weight location.

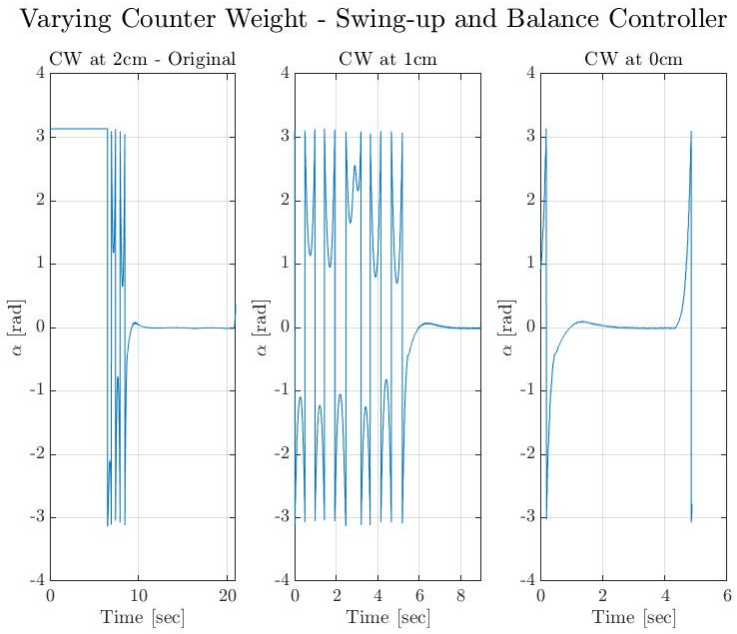

Figure 21: Varying location of counter weight - Swing-up and Balance Controller. The impact of varying the location of counter weight was analyzed by changing the location of the counter weights for a fully controlled system. The system was only able to balance from 0 to 2cm from end of the horizontal link.

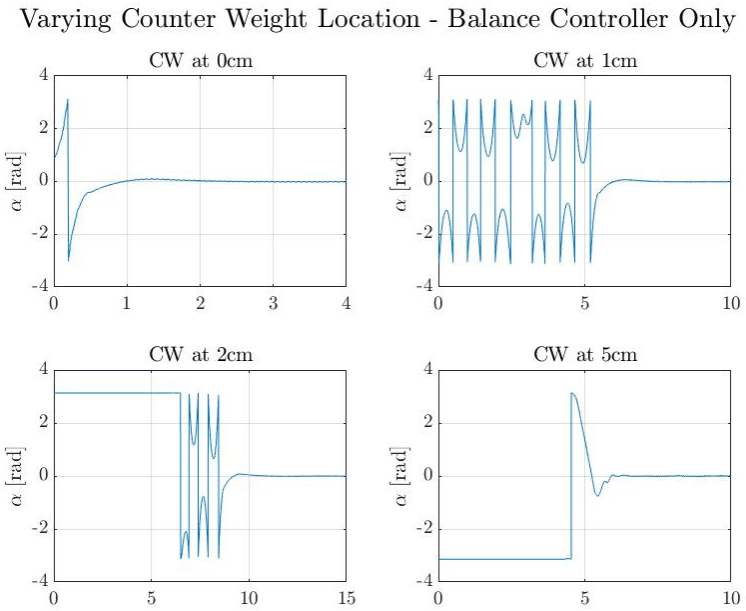

Figure 22: Varying location of counter weight for Balance Controller only. The impact of varying the location of counter weight was analyzed by changing the location of counter weights. System was able balance at the maximum displacement range of the counter weight.

7 Effect of Loop Rate (10pts)

The cycle time is set at $5ms$ for the LabVIEW environment and $1ms$ for the Simulink environment. To determine the effect of cycle time on the system, it is gradually increased from $5ms$ until the system starts behaving erratically.

(a) Balance the System (5)

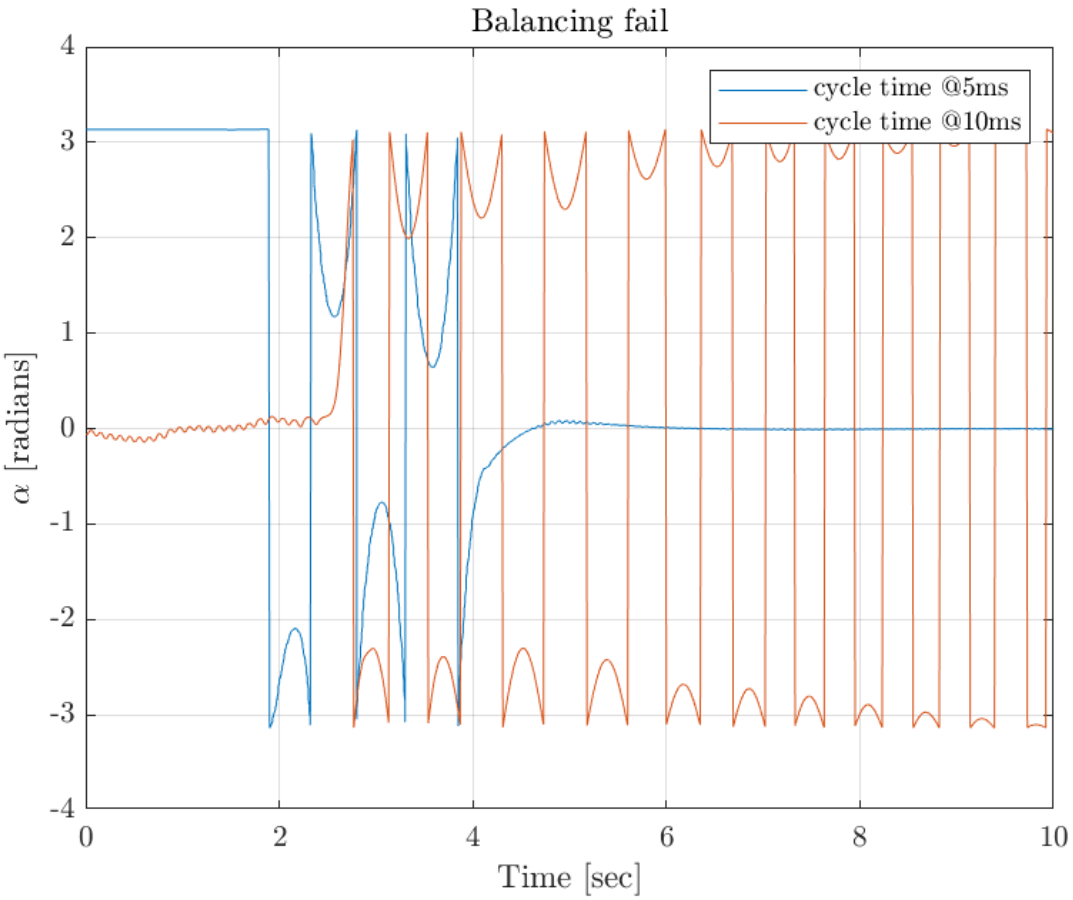

Figure 23: Effect of loop rate on balancing the system

The pendulum is manually held at the top position and the system is then started, but as shown in figure 23 the balancing controller fails at a cycle time of $10ms$.

(b) Swing-up the System (5)

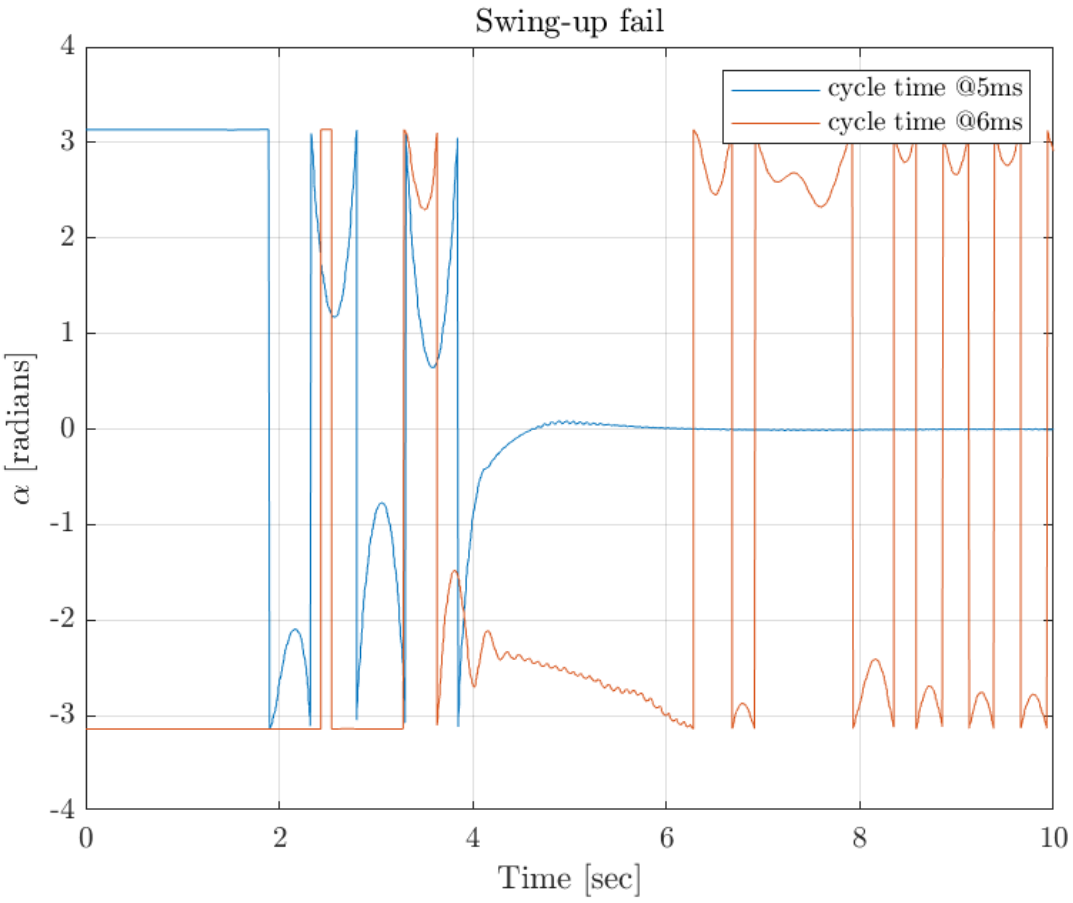

Figure 24: Effect of loop rate on swing-up the system

For testing the effect of cycle time on the swing-up control, the system is allowed to swing up from the bottom down rest position ($\alpha = \pi$). The swing-up controller tries to swing up but fails to do so as can be seen in figure 24.

In comparison to the balancing controller (which eventually fails when the cycle time is set at $10ms$), the swing-up control starts to fail even at $6ms$. This happens because of two major reasons, one of them being the high non-linearity in the swing-up region, which is then aggravated by minimizing the amount of data collection by increasing the loop cycle time.

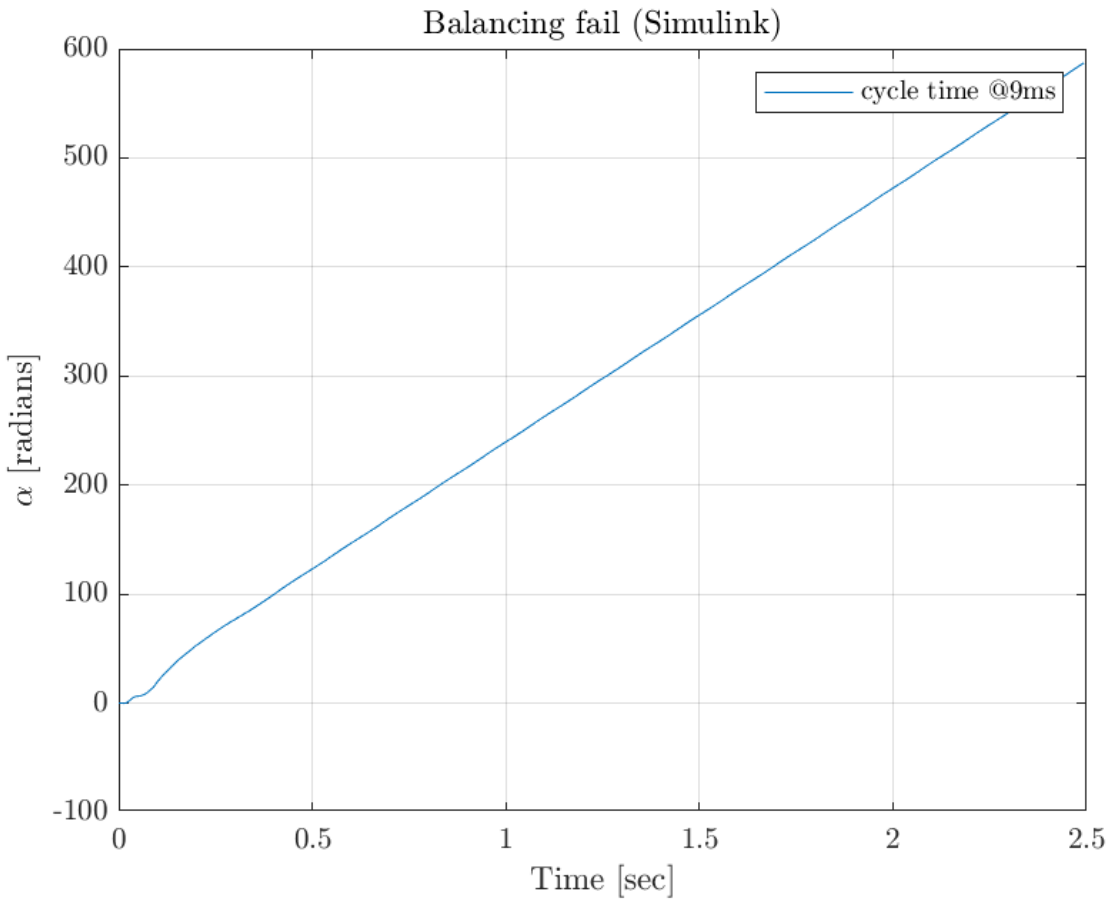

Figure 25: Effect of loop rate on balancing the system on Simulink

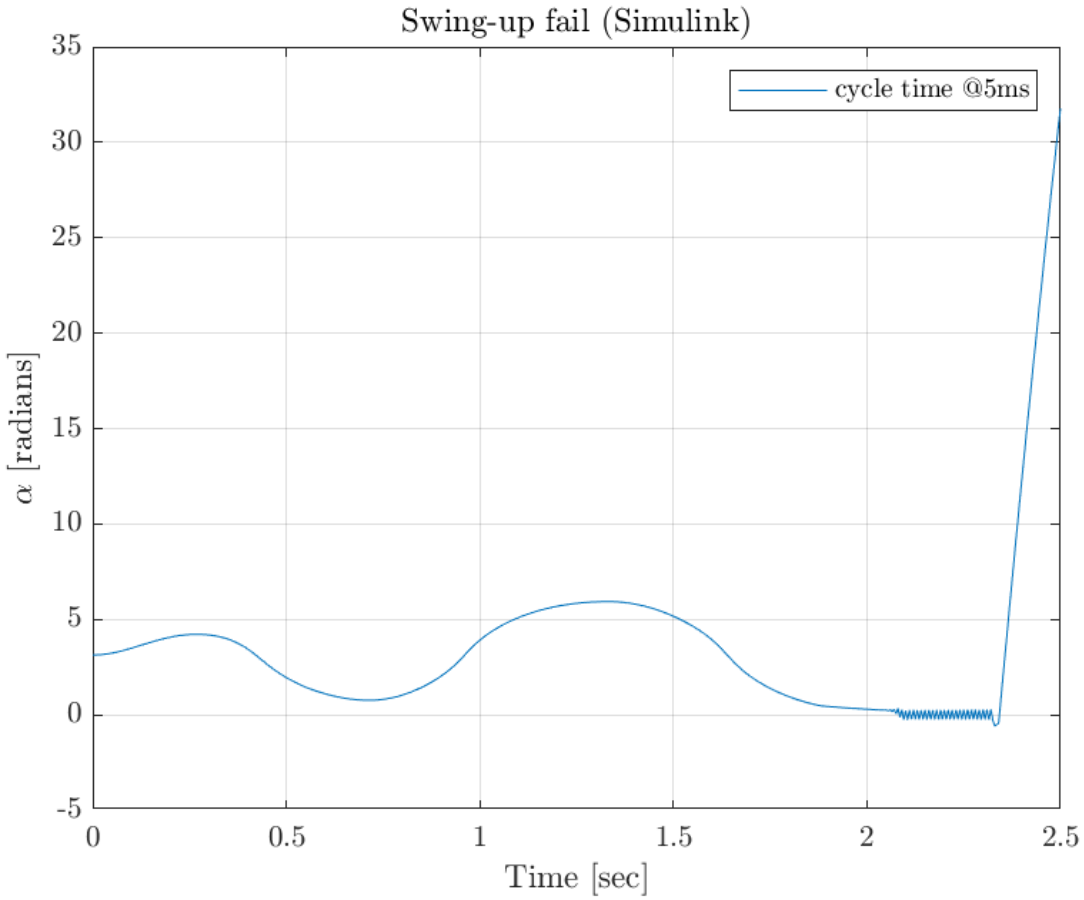

Figure 26: Effect of loop rate on swing-up the system on Simulink

Similar results are obtained from changing the loop cycle time in Simulink. The balancing controller is initialised with α as 0.001 radians and allowed to balance on its own. The system fails to balance when the loop cycle time is set at $9ms$ which is similar to the loop cycle time obtained experimentally ($10ms$). Similarly, the swing-up control is initialized with α as π and allowed to swing up and stabilise. The system starts failing at a loop cycle time of $5ms$, which is close to the experimental value of $6ms$.

8 Balancing Controller — Classical Approach (24pts)

(a) Controller Design (10)

(b) Controller Performance Simulation (7)

(c) Controller Implementation (7)

References

[1] Friction & Frequency Factors. Retrieved from https://www.amroll.com/friction-frequency-factors.html

Appendix A: Source Code

Listing 1: MATLAB code for parameter identification.

```
%% Friction Torque And Inertia Of Horizontal Arm

data = HorizontalArmnewParamID90deg.AmplitudePlot0;
times =  HorizontalArmnewParamID90deg.TimePlot0;
data = data(2359:end);
times = times(2359:end);
m = 0.14988;%
%Distance of CG from pivot (m)
r = 0.037633;
g = 9.81; %m/s2
J = 0.00071866;
dist = 10;
[tops, locT] = findpeaks(data, 'MinPeakDistance', dist);
[bots, locB] = findpeaks(-1.*data, 'MinPeakDistance', dist);
tops = tops(1:end);
locT = locT(1:end);
theta_difT = mean(tops(2:end)-tops(1:end-1));
theta_difB = mean(bots(2:end)-bots(1:end-1));
theta_dif = mean([theta_difT theta_difB]);
f = fit(times(locT), data(locT), 'exp1');
delta = -1*f.b;
figure();
hold on
plot(times, data, 'LineWidth',2);
% plot(times(locT), data(locT));
% plot(times(locB), data(locB));
Tf = m*g*r*theta_dif/4; %Newtons
p  =polyfit(times(locT(1:end-4)), data(locT(1:end-4)), 1);
vals2 = polyval(p, times(locT(1:end-4)));
plot(times(locT(1:end-4)), vals2, 'LineWidth',2)
zero_crossings = [];

freq = 8.976;
J = (m*g*r)/(freq^2);
%Damping ratio
zeta = delta/sqrt(delta^2 + (2*pi)^2);
%Viscous damping coefficient (N-m-s)
B = 2*zeta*freq*J;
plot(f)
xlabel('Time (sec)','interpreter','latex');
ylabel('$\theta$ [rad]','interpreter','latex');
title('Horizontal Link ID','interpreter','latex');
grid on
set(gca,'ticklabelinterpreter','latex');
```

```
box on
saveas(gca,'FrTorque.png');

%% Friction And Inertia Of Pendulum
data = PendulumnewParamIDFinal.AmplitudePlot0;
times =  PendulumnewParamIDFinal.TimePlot0;
data = data(780:end);
times = times(780:end);
cut = 4000;
lintimes = times(cut:end);
lindata = data(cut:end);



g = 9.81;
%Mass of link (kg)
m = 0.077;%
%Distance of CG from pivot (m)
r = 0.084;
%Inertia about pivot (kg-m2)
%J = m*9.81*r/wn^2;
%Inertia about CG (kg-m2)


%Amplitude attenuation\
dist = 10;
[tops, locT] = findpeaks(data(1:cut), 'MinPeakDistance', dist);
[bots, locB] = findpeaks(-1.*data(1:cut), 'MinPeakDistance', dist);
tops = tops(2:end);
locT = locT(2:end);
%wn =1/( median(times(locT(2:end))-times(locT(1:end-1))));
freq = (2*pi)/(13.26-12.45);
deltaT = log(tops(1:end-3)./tops(2:end-2));
%deltaB = log(bots(1:end-3)./bots(2:end-2));
delta = mean(deltaT) ;
f = fit(times(locT), data(locT), 'exp1');
delta = -1*f.b;
J = (m*g*r)/(freq^2);
J_o = J - m*r^2;
figure();
hold on
plot(times,data,'LineWidth',2);


plot(f)
%Damping ratio
zeta = delta/sqrt(delta^2 + (2*pi)^2);
```

```
%Viscous damping coefficient (N-m-s)
B = 2*zeta*freq*J;

[linPeaks, linlocs] = findpeaks(lindata, 'MinPeakDistance', dist);
theta_dif = median(linPeaks(1:end-1)-linPeaks(2:end));
p  =polyfit(times(linlocs+cut), data(linlocs+cut), 1);
vals2 = polyval(p, times(linlocs+cut));
plot(times(linlocs+cut), vals2, 'LineWidth',2)
Tf = m*g*r*theta_dif/4; %Newtons
xlabel('Time (sec)','interpreter','latex');
ylabel('$\theta$ [rad]','interpreter','latex');
title('Pendulum ID','interpreter','latex');
grid on
set(gca,'ticklabelinterpreter','latex');
box on
saveas(gca,'pendulumFriction.png');
```

Listing 2: MATLAB code for computing $\ddot{\theta}$ as in figure 4.

```
function thetaddot = fcn(u,T)
%%parameter list
L1 = 0.2032;
L11 = -0.01;
L21 = 0.0827;
m1 = 0.1707; %[kg]
m2 = 0.0787; %[kg]
i1 = 7.1866E-4;
i2 = [0.0009 0 8.8E-7; 0 0.00091121 0; 0 0 1.033E-5];
B_theta = 0;
B_alpha = 1.3985E-4;
T_falpha = 2.7455E-4;
T_ftheta = 1.98E-3;
g=9.81;

td = u(2);
a = u(4);
ad = u(5);
add = u(6);

coeff1 = m1*L11^2+i1+m2*L1^2+m2*L21^2*sin(a)^2+i2(1,1)*sin(a)^2+i2
   (2,2)*cos(a)^2;
coeff2 = (i2(1,2)-m2*L1*L21)*cos(a)*add;
coeff3 = (i2(2,2)-m2*L1*L21)*sin(a)*ad^2;
coeff4 = (i2(3,3)+m2*L21^2-i2(2,2))*(2*cos(a)*sin(a))*(ad*td);
thetaddot = (T - (B_theta*td+T_ftheta*sign(td))+coeff2-coeff3-coeff4
   )/coeff1;
```

Listing 3: MATLAB code for computing $\ddot{\alpha}$ as in figure 4.

```
function alphaddot = fcn(u)
%%parameter list
L1 = 0.2032;
L11 = -0.01;
L21 = 0.0827;
m1 = 0.1707; %[kg]
m2 = 0.0787; %[kg]
i1 = 7.1866E-4;
i2 = [0.0009 0 8.8E-7; 0 0.00091121 0; 0 0 1.033E-5];
B_theta = 0;
B_alpha = 1.3985E-4;
T_falpha = 2.7455E-4;
T_ftheta = 1.98E-3;
g=9.81;

td = u(2);
tdd = u(3);
a = u(4);
ad = u(5);

coeff1 = m2*L21^2+i2(1,1);
coeff2 = i2(1,2)-m2*L1*L21*cos(a)*tdd;
coeff3 = m2*L21^2-i2(2,2)+i2(1,1)*(cos(a)*sin(a))*td^2;
coeff4 = m2*g*L21*sin(a);
alphaddot = (B_alpha*ad+T_falpha*sign(ad)-coeff2-coeff3-coeff4)/(-
   coeff1);
```

Appendix B: Parameter Identification

- Gravity, g: A universal constant
- Length of Horizontal Arm, L_1: Measured in cad; the distance between one short side of the horizontal arm to the other
- Distance of the Horizontal Arms Center of Mass from its pivot point at O, L_{11}: measured in CAD by creating a coordinate system with an origin at O and then evaluating the horizontal link assemblies mas properties in relation to the created coordinate system.
- Mass of Horizontal Arm, M_1: the counter-weight, pendulum encoder, and horizontal arm were weighed together. The mass was compared to the same set of items in CAD and then the mass of the pendulum encoder shaft was subtracted. [Does this need the motor mass as well?]
- Moment of Inertia of the Horizontal Arm Assembly about its Center of Mass and aligned with the O coordinate system, I_{1,z_O}: measured in CAD by creating a coordinate

system with an origin at O and then evaluating the horizontal link assemblies mas properties in relation to the created coordinate system.

- Friction Torque for Direction θ, $T_{f,\theta}$: measured experimentally by calculating $\frac{M_1 * g * L_{11}}{4}(\theta_{n-1} - \theta_n)$ successively for each peak of the linear decay region of the oscillation and then averaging those values. Since the entire oscillation decayed linearly, all the peaks were used.

- Viscous Damping for Direction θ, B_θ: As mentioned in the previous point, the oscillations decayed linearly for the entire data set. This indicated that there was a negligible amount of viscous damping for θ.

- Back EMF Constant for Motor, K_b: taken from the motor datasheet

- Torque Constant for Motor, K_t: taken from the motor datasheet

- Motor Resistance, R: taken from the motor datasheet

- Motor Inductance, L: taken from the motor datasheet

- Motor Viscous Damping Constant, B_m : taken from the motor datasheet

- Friction Torque for Motor, $T_{f,motor}$: taken from the motor datasheet

- Motor Inertia, J_m: taken from the motor datasheet

- Length of Pendulum Arm, L_2: measured in CAD

- Distance Of Pendulum Arm CoM from Pivot,L_{21}: found in CAD by creating a coordinate system with its origin at the the pivot point of the pendulum, then evaluating the mass properties in relation to that point

- Mass of Pendulum Arm, M_2: mass of the pendulum assembly sans the parts in the encoder assembly, the mass was compared to the respective parts in CAD and then the mass of the entire pendulum assembly was pulled from the CAD with the appropriate adjustments

- Moment of Inertia of Pendulum at its Center of Mass and aligned with B_X, I_{2,B_X}: found from CAD by creating a coordinated system with its origin at point B and then evaluating the mass properties in relation to that coordinate system. This value was verified experimentally as described below.

- Moment of Inertia of Pendulum at its Center of Mass and aligned with B_Y, I_{2,B_Y}: found from CAD by creating a coordinated system with its origin at point B and then evaluating the mass properties in relation to that coordinate system.

- Moment of Inertia of Pendulum at its Center of Mass and aligned with B_Z, I_{2,B_Z}: found from CAD by creating a coordinated system with its origin at point B and then evaluating the mass properties in relation to that coordinate system.

- Product of Inertia of Pendulum aligned with B_{XY}, $I_{2,B_{XY}}$: found from CAD by creating a coordinated system with its origin at point B and then evaluating the mass properties in relation to that coordinate system.

- Friction Torque for Direction α, $T_{f,\alpha}$: data found experimentally as described below with the formula $\frac{M_1 * g * L_{11}}{4}(\alpha_{n-1} - \alpha_n)$ evaluated on the peaks of the linear decay region of the oscillations.

- Viscous Damping for Direction α, B_α: data found experimentally as described below. An exponential fit was applied to the peaks of the exponential region and the the δ value from the fit was applied to the formula $\zeta = \frac{\delta}{\sqrt{delta^2 + (2*\pi)^2}}$. And finally $B = 2 * \zeta \omega_n^2 * J_P$, where J_P is the pendulum's inertia about its pivot.

In order to validate the various CAD derived values we used, we performed two similar experiments. The first was that we removed the pendulum arm from the assembly, placed the horizontal link and motor assemblies on their side, brought the horizontal link to a parallel position with the ground, and then let it swing while the motor encoder measurements were recorded by the myRio. In our first attempt of this experiment we used the original configuration of the horizontal link and motor assembly, but due to the counter-weight and friction from the motor, there were few to no oscillations. Removing the counter-weight to increase the moment did increase the number of oscillations, but only marginally. Finally, we decided to tape the counter-weight on the same end of the horizontal arm as the encoder arm, but on the opposite face. This configuration produced a satisfactory number of oscillations but produced another hurdle in that the values of inertia, friction, etc. that we were trying to measure from this experiment were not representative of our operating configuration. The inertia the value we derived from our experiment was necessarily different than the operating configuration, but we were still able to validate the inertia values from CAD by building an assembly that matched our experimental configuration and comparing that to our experimental value. The viscous friction value should not change between configurations because it is a property of how the balls of the bearing move through the lubricant which does not change between configurations. The friction torque of a bearing is proportional to the load by a small(10^{-3}[1]) coefficient of friction. This means that the assembly being on its side as well as the increased mass should create a discrepancy between the friction torque we derive through this experiment($0.0015 Nm$) versus the one the horizontal link experiences during operation. It is also possible that the link experiences more friction during operation due to the centrifugal forces. And as described in section 3, we do find that a different friction torque improves our model. From this experiment we found an inertia value of 6.87E-4 $kg * m^2$, which validates the value we used from CAD of 7.28E-4 $kg * m^2$.

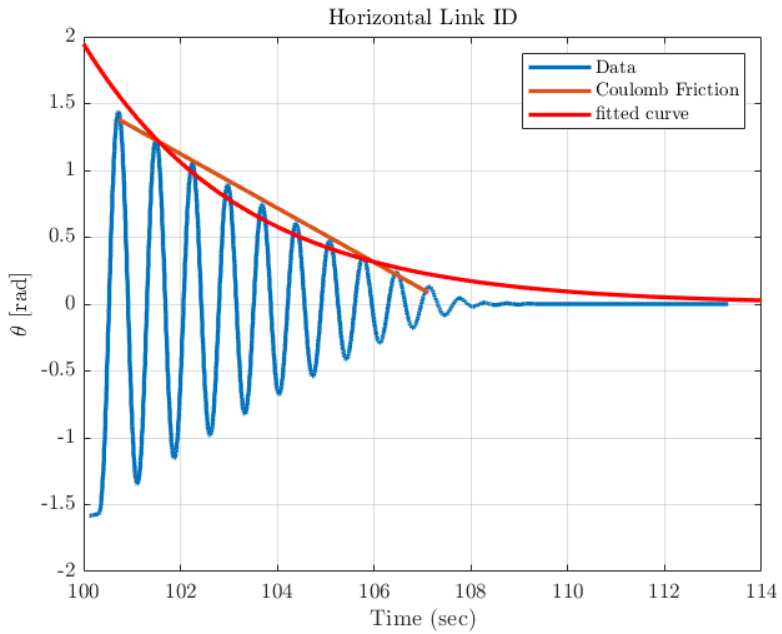

Figure 27: Oscillation Data collected for the horizontal link. The lack of exponential decay region suggests a lack of contribution from the viscous damping. The exponential fit highlights this fact.

In the second experiment we detached the horizontal link, fixed it to a table, and then let the pendulum arm swing as its encoder values were recorded. In this experiment there were no conflicts of configuration and we were able to again validate our CAD derived values. We were able to measure the inertia about the pivot experimentally and compare that value, 0.0011, to the value found from CAD, 0.0009. The inertia was calculated via: Inertia of Pendulum about pivot, $J_P = \frac{g*M_2L_{21}}{\omega_n^2}$.

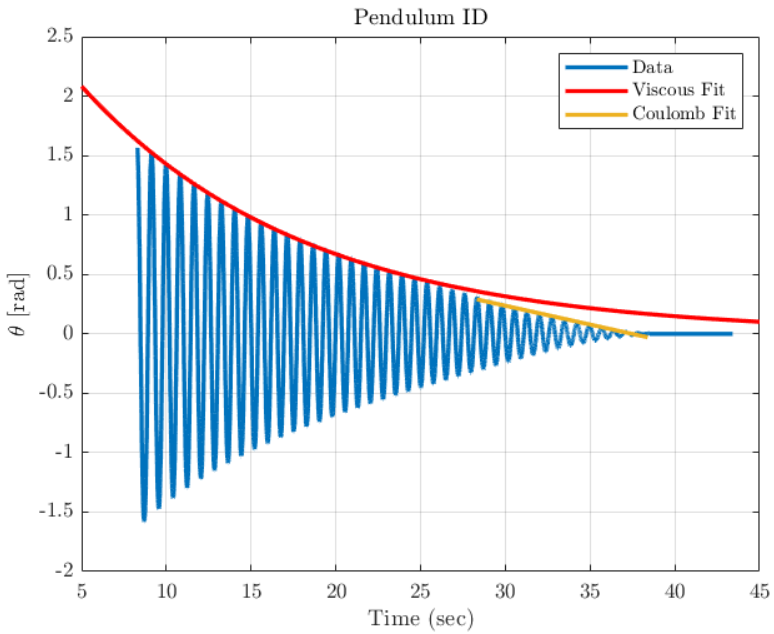

Figure 28: Oscillation Data collected for the pendulum link. The viscous damping constant value is derived from the exponential decay region while the coulomb friction is derived from the linear decay region.